Gas adsorption and desorption in silica aerogels: A theoretical study of scattering properties

F. Detcheverry, E. Kierlik, M. L. Rosinberg, and G. Tarjus
Laboratoire de Physique Théorique de la Matière Condensée, Université Pierre et Marie Curie, 4 Place Jussieu, 75252 Paris Cedex 05, France
(Received 18 October 2005; published 19 April 2006)

We present a numerical study of the structural correlations associated with gas adsorption and desorption in silica aerogels in order to provide a theoretical interpretation of scattering experiments. Following our earlier work, we use a coarse-grained lattice-gas description and determine the nonequilibrium behavior of the adsorbed gas within a local mean-field analysis. We focus on the differences between the adsorption and desorption mechanisms and their signature in the fluid-fluid and gel-fluid structure factors as a function of temperature. At low temperature, but still in the regime where the isotherms are continuous, we find that the adsorbed fluid density, during both filling and draining, is correlated over distances that may be much larger than the gel correlation length. In particular, extended fractal correlations may occur during desorption, indicating the existence of a ramified cluster of vapor filled cavities. This also induces an important increase of the scattering intensity at small wave vectors. The similarity and differences with the scattering of fluids in other porous solids such as Vycor are discussed.

DOI: 10.1103/PhysRevE.73.041511 PACS number(s): 64.70.Fx, 75.60.Ej, 61.20.Gy, 67.70.+n

I. INTRODUCTION

In a series of recent papers [1–3], we have presented a comprehensive theoretical study of gas adsorption and desorption in silica aerogels, revealing the microscopic mechanisms that underly the changes in the morphology of the hysteresis loops with temperature and gel porosity. In particular, we have shown that the traditional capillary condensation scenario based on the independent-pore model [4] does not apply to aerogels, as a consequence of the "open" nature and interconnectedness of their microstructure. We have found, on the other hand, that nonequilibrium phase transitions (that differ on adsorption and desorption) are at the origin of the very steep isotherms observed with ^{4}He in high porosity gels at low temperature [5,6]. In this work, we complete our study by investigating the correlations within the adsorbed fluid and computing the fluid-fluid and solid-fluid structure factors that can be measured (at least indirectly) in scattering experiments. Scattering methods (using x rays, neutrons, and visible light) are now frequently combined with thermodynamic measurements for extracting information on the structure and the dynamics of the adsorbed molecules and understanding the influence of solid microstructure on fluid properties [7]. In the case of ^{4}He in aerogel, both small-angle x-ray scattering (SAXS) [8] and light scattering measurements [9] have been recently performed along the sorption isotherms. However, the interpretation of the scattered intensity is always complicated by the fact that it contains several contributions that cannot be resolved without assuming some mechanism for the sorption process. For instance, in the case of a low porosity solid like Vycor, the evolution of the scattered intensity along the capillary rise is usually interpreted in the framework of an independent-pore model, with the gas condensing in pores of increasing size that are (almost) randomly distributed throughout the material [10–12]. This explains that long-range correlations are not observed during adsorption. On the other hand, we have shown that large-scale collective events occur in aerogels, and this may have a significant influence on the scattering properties. Indeed, we shall see in the following that scattering curves at low temperature may not reflect the underlying microstructure of the gel. More generally, our main objective is to understand how the different mechanisms for adsorption and desorption reflect in the scattering properties as the temperature is changed. (Note that there has been a recent theoretical study of this problem that is closely related to the present one [13]; there are, however, significant differences that will be commented in due place.) Particular attention will be paid to the "percolation invasion" regime that is predicted to occur during the draining of gels of medium porosity (e.g., 87%) and that manifests itself by the presence of fractal correlations. Such correlations have been observed in Vycor [10–12] and xerogel [14], but no experiment has been carried out so far to detect a similar phenomenon in aerogels. We therefore hope that the present work will be an incentive for such a study. On the other hand, the influence of gel porosity on scattering properties will only be evoked very briefly. In particular, for reasons that will be explained below, the correlations along the steep (and possibly discontinuous due to nonequilibrium phase transitions) isotherms observed in high porosity gels at low temperature are not investigated.

The paper is organized as follows: In Sec. II, the model and the theory are briefly reviewed and the computation of the correlation functions and the corresponding structure factors is detailed. The numerical results are presented in Sec. III. The relevance of our results to existing and future scattering experiments is discussed in Sec. IV.

II. MODEL AND CORRELATION FUNCTIONS

A. Lattice-gas model

As discussed in previous papers [1–3], our approach is based on a coarse-grained lattice-gas description which in-

 ©2006 The American Physical Society

corporates the essential physical ingredients of gel-fluid systems. The model Hamiltonian is given by

$$\mathcal{H} = -w_{ff}\sum_{\langle ij\rangle}\tau_i\tau_j\eta_i\eta_j - w_{gf}\sum_{\langle ij\rangle}[\tau_i\eta_i(1-\eta_j)+\tau_j\eta_j(1-\eta_i)] - \mu\sum_i \tau_i\eta_i, \quad (1)$$

where $\tau_i=0,1$ is the fluid occupation variable ($i=1,\ldots,N$) and $\eta_i=1,0$ is the quenched random variable that describes the solid microstructure [when $\eta_i=0$, site i is occupied by the gel; $\phi=(1/N)\Sigma_i\eta_i$ is thus the gel porosity]. Specifically, we address the case of base-catalyzed silica aerogels (typically used in helium experiments) whose structure is well accounted for by a diffusion limited cluster-cluster aggregation algorithm (DLCA) [15]. In the Hamiltonian, w_{ff} and w_{gf} denote respectively the fluid-fluid and gel-fluid attractive interactions, μ is the fluid chemical potential (fixed by an external reservoir), and the double summations run over all distinct pairs of nearest-neighbor (n.n.) sites.

Fluid configurations along the sorption isotherms are computed using local mean-field theory (i.e., mean-field density functional theory), neglecting thermal fluctuations and activated processes (the interested reader is referred to Refs. [1–3] for a detailed presentation of the theory). As μ varies, the system visits a sequence of metastable states which are local minima of the following grand-potential functional;

$$\Omega(\{\rho_i\}) = k_BT\sum_i[\rho_i\ln\rho_i + (\eta_i-\rho_i)\ln(\eta_i-\rho_i)] - w_{ff}\sum_{\langle ij\rangle}\rho_i\rho_j - w_{gf}\sum_{\langle ij\rangle}[\rho_i(1-\eta_j)+\rho_j(1-\eta_i)] - \mu\sum_i\rho_i, \quad (2)$$

where $\rho_i(\{\eta_i\})=\langle\tau_i\eta_i\rangle$ is the thermally averaged fluid density at site i. Earlier work has shown that this approach reproduces qualitatively the main features of adsorption phenomena in disordered porous solids [16,17].

All calculations presented below were performed on a body-centered cubic lattice of linear size $L=100$ ($N=2L^3$) with periodic boundary conditions in all directions (the lattice spacing a is taken as the unit length). L is large enough to faithfully describe gels with porosity $\phi\leqslant 95\%$, but an average over a significant number of gel realizations is required to obtain a good description of the correlation functions. In the following, we use 500 realizations. w_{ff} is taken as the energy unit and temperatures are expressed in the reduced unit $T^*=T/T_c$, where T_c is the critical temperature of the pure fluid ($T_c=5.195$ K for helium and $kT_c/w_{ff}=2$ in the theory). The interaction ratio $y=w_{gf}/w_{ff}$ is equal to 2 so as to reproduce approximately the height of the hysteresis loop measured with ^{4}He in a 87% porosity aerogel at $T=2.42$ K [1,6].

B. Correlation functions and structure factors

In a scattering experiment performed in conjunction with gas adsorption and desorption, one typically measures a (spherically averaged) scattered intensity $I(q)$ which is proportional to a combination of the three partial structure factors $S_{gg}(q)$, $S_{ff}(q)$, and $S_{gf}(q)$, where g and f denote the gel and the fluid, respectively. Whereas a macroscopic sample is usually considered as isotropic and statistically homogeneous, our calculations are performed in finite samples and on a lattice, and some work is needed to obtain structure factors that can be possibly compared to experimental data.

Let us first consider the gel structure factor. The calculation of $S_{gg}(q)$ proceeds in several steps. As in the case of an off-lattice DLCA simulation [18], we first compute the two-point correlation function $g_{gg}(\mathbf{r})=h_{gg}(\mathbf{r})+1$ by performing a double average over the lattice sites and the gel realizations,

$$\rho_g^2 g_{gg}(\mathbf{r}) = \frac{1}{N}\sum_{i,j}\overline{(1-\eta_i)(1-\eta_j)}\,\delta_{\mathbf{r},\mathbf{r}_{ij}} - \rho_g\delta_{\mathbf{r},\mathbf{0}} \quad (3)$$

taking care of the periodic boundary conditions. Here, $\mathbf{r}_{ij}=\mathbf{r}_i-\mathbf{r}_j$, $\rho_g=1-\phi$ is the lattice fraction occupied by the gel, and the second term in the right-hand side takes into account the fact that there are only one particle per site, which yields the (point) hard-core condition, $g_{gg}(\mathbf{r}=\mathbf{0})=0$. In this expression and in the following, the overbar denotes an average over different gel realizations produced by the DLCA algorithm. The computation of $g_{gg}(\mathbf{r})$ is performed by introducing the Fourier transform of the one-body density, $\rho_g(\mathbf{q})=\Sigma_i(1-\eta_i)\exp(-2i\pi\mathbf{q}.\mathbf{r_i}/N)$, where $\mathbf{q}$ is a vector of the reciprocal lattice; the average over the gel realizations of the product of $\rho_g(\mathbf{q})$ by its conjugate is then the Fourier transform of $g_{gg}(\mathbf{r})$, and one can use the efficient fast Fourier transform (FFT) method to compute $\rho_g(\mathbf{q})$ [13,19]. This reduces the computational work to $O(N\ln N)$ instead of $O(N^2)$ when the direct real-space route is used. (The same method is applied to the other correlation functions.)

In a second step, we "sphericalize" the correlation function by collecting the values having same modulus of the argument $\mathbf{r}$,

$$g_{gg}(r) = \frac{\sum_{\mathbf{r}'} g_{gg}(\mathbf{r}')\,\delta_{r,r'}}{\sum_{\mathbf{r}'}\delta_{r,r'}}. \quad (4)$$

Finally, instead of storing the values of $g_{gg}(r)$ for all possible distances r_{ij} on the lattice between $d=a\sqrt{3}/2$, the nearest-neighbor distance, and $L/2$, we bin the data with a spacing $\Delta r=0.05$ and interpolate linearly between two successive points (the restriction to $r<L/2$ avoids boundary artefacts). Moreover, we impose the "extended" hard-core condition $g_{gg}(r)=0$ for $r<d$, in line with our interpretation of a gel site as representing an impenetrable silica particle [1]. (In Ref. [13], in contrast, the model is thought of as a discretization of space into cells of the size of a fluid molecule and the gel particle "radius" is varied from 2 to 10 lattice spacings.) Of course, the interpolation procedure does not completely erase the dependence on the underlying lattice structure, especially at short distances. Following Ref. [18], the structure factor is then computed using

$$S_{gg}(q) = 1 + 4\pi\rho_g\int_0^{L/2} r^2(h_{gg}(r)-h_{gg})\frac{\sin(qr)}{qr}dr, \quad (5)$$

where h_{gg} is a very small parameter adjusted such that $S_{gg}(q)\to 0$ as $q\to 0$. Indeed, since the DLCA aerogels are

built in the "canonical" ensemble with a fixed number of gel particles $N_g=\rho_g N$, the following sum-rule holds:

$$\rho_g \sum_{\mathbf{r}} g_{gg}(\mathbf{r}) = N_g - 1 \tag{6}$$

which readily yields $S_{gg}(0)=1+\rho_g \Sigma_{\mathbf{r}} h_{gg}(\mathbf{r})=0$ in Fourier space. This trick allows one to obtain a reasonable continuation of $S_{gg}(q)$ below $q_{\min}=2\pi/L$ [18].

Similarly, the fluid-fluid two-point correlation function $g_{ff}(\mathbf{r})=1+h_{ff}(\mathbf{r})$ is defined as

$$\rho_f^2 g_{ff}(\mathbf{r}) = \frac{1}{N}\sum_{i,j} \overline{\langle \tau_i \eta_i \tau_j \eta_j \rangle} \delta_{\mathbf{r},\mathbf{r}_{ij}} - \rho_f \delta_{\mathbf{r},\mathbf{0}}, \tag{7}$$

where $\rho_f=(1/N)\Sigma_i \overline{\langle \tau_i \eta_i \rangle}=(1/N)\Sigma_i \overline{\rho_i}$ is the average fluid density and the sum is performed again over all lattice sites to improve the statistics (for notational simplicity, we have dropped the overbar on ρ_f). Because of the double average over thermal fluctuations and over disorder, there are two distinct contributions to $h_{ff}(\mathbf{r})$, which are usually called "connected" and "blocking" or "disconnected" [20,21], and which, in the present case, are given by the expressions,

$$\rho_f^2 h_{ff,c}(\mathbf{r}) + \rho_f \delta_{\mathbf{r},\mathbf{0}} = \frac{1}{N}\sum_{i,j} \overline{[\langle \tau_i \eta_i \tau_j \eta_j \rangle - \rho_i \rho_j]} \delta_{\mathbf{r},\mathbf{r}_{ij}}, \tag{8}$$

$$\rho_f^2 h_{ff,d}(\mathbf{r}) = \frac{1}{N}\sum_{i,j} [\overline{\rho_i \rho_j} - \rho_f^2] \delta_{\mathbf{r},\mathbf{r}_{ij}}. \tag{9}$$

In the pure fluid, $h_{ff,c}(\mathbf{r})$ is just the standard connected pair correlation function whereas $h_{ff,d}(\mathbf{r})$ has no equivalent. It turns out, however, that only $h_{ff,d}(\mathbf{r})$ can be computed along the sorption isotherms. Indeed, the quantity $\langle \tau_i \eta_i \tau_j \eta_j \rangle$ cannot be obtained in the framework of mean-field theory, and the only available route to $h_{ff,c}(\mathbf{r})$ is via the "fluctuation" relation [21]

$$\rho_f^2 h_{ff,c}(\mathbf{r}_{ij}) + \rho_f \delta_{\mathbf{r}_{ij},\mathbf{0}} = \frac{\partial^2 \beta\Omega}{\partial(\beta\mu_i)\partial(\beta\mu_j)} = \frac{\partial \rho_i}{\partial(\beta\mu_j)}, \tag{10}$$

where μ_i is a site-dependent chemical potential [22]. However, this relation only holds at equilibrium (like the Gibbs adsorption equation $\rho_f=-(1/N)\partial\Omega/\partial\mu$ discussed in Ref. [1]) and therefore it cannot be applied along the hysteresis loop where the system jumps from one metastable state to another. (In a finite sample, the grand potential changes discontinuously along the adsorption and desorption desorption branches [1].) We are thus forced to approximate $h_{ff}(\mathbf{r})$ by its disconnected part, $h_{ff,d}(\mathbf{r})$ [23]. However, this may not be a bad approximation at low temperature because the local fluid densities ρ_i are then very close to zero or one [1], which likely implies that $h_{ff,c}(\mathbf{r})$ is a much smaller quantity than $h_{ff,d}(\mathbf{r})$ [24].

We then apply to $h_{ff}(\mathbf{r})$ the same procedure as for $g_{gg}(\mathbf{r})$, taking radial averages and then performing a binning of the data and a linear interpolation. There are no "extended" hard-core in this case. Indeed, since the scale of the coarse-graining is fixed by the size of a gel particle (typically, a few nanometers), a lattice cell may contain several hundreds of fluid molecules which may be thus considered as point particles. $h_{ff}(r)$ is then also interpolated between $r=0$ and $r=d$.

In a grand-canonical calculation, the number of fluid particles fluctuates from sample to sample, which implies the following sum-rule for the disconnected pair correlation function $h_{ff,d}(\mathbf{r})$ [21] [and thus for $h_{ff}(\mathbf{r})$ in our approximation]

$$\sum_{\mathbf{r}} h_{ff}(\mathbf{r}) \simeq \sum_{\mathbf{r}} h_{ff,d}(\mathbf{r}) = N\frac{\overline{\rho_f^2(\{\eta_i\})} - \rho_f^2}{\rho_f^2}, \tag{11}$$

where $\rho_f(\{\eta_i\})=(1/N)\Sigma_i \rho_i$ is the average fluid density for a given gel realization. This sum rule can be used to also extrapolate $S_{ff}(q)$ below $q<2\pi/L$, using

$$S_{ff}(q) = 1 + 4\pi\rho_f \int_0^{L/2} r^2 (h_{ff}(r) - h_{ff}) \frac{\sin(qr)}{qr} dr, \tag{12}$$

where h_{ff} is adjusted so that $S_{ff}(0)=1+N[\overline{\rho_f^2(\{\eta_i\})}-\rho_f^2]/\rho_f$.

Finally, the gel-fluid two-point correlation function $g_{gf}(\mathbf{r})=1+h_{gf}(\mathbf{r})$ is computed from

$$\rho_g \rho_f g_{gf}(\mathbf{r}) = \frac{1}{N}\sum_{i,j} \overline{(1-\eta_i)\langle \tau_j \eta_j \rangle} \delta_{\mathbf{r},\mathbf{r}_{ij}} \tag{13}$$

and then sphericalized, binned, and linearly interpolated [taking $g_{gf}(r)=0$ for $0<r<d/2$ since no fluid molecule can be found at a distance less than $d/2$ from the centre of a gel particle]. The cross structure factor $S_{gf}(q)$ is then obtained from

$$S_{gf}(q) = 4\pi\sqrt{\rho_g \rho_f} \int_0^{L/2} r^2 (h_{gf}(r) - h_{gf}) \frac{\sin(qr)}{qr} dr, \tag{14}$$

where h_{gf} is adjusted so as to satisfy the sum rule $S_{gf}(q \to 0)=0$ which again results from the absence of fluctuations in the number of gel particles.

III. NUMERICAL RESULTS

A. Aerogel structure

We first concentrate on the case of the empty aerogel. We have already presented in Ref. [1] the pair correlation function $g_{gg}(r)$ for several porosities between 87% and 99%. These curves exhibit a shallow minimum that strongly depends on ϕ and whose position gives an estimate of the gel correlation lenght ξ_g, as suggested in Ref. [18]. A DLCA gel can indeed be sketched as a disordered packing of ramified blobs with average size ξ_g. For instance, ξ_g varies approximately from 4 to 10 lattice spacings as the porosity increases from 87% to 95% (this is much smaller than the box size L, which ensures that there are no finite-size artifacts in the calculation of the gel structure [25]). Only the highest-porosity samples exhibit a significant power-law regime $g_{gg}(r) \sim r^{-(3-d_f)}$ that reveals the fractal character of the intrablob correlations. Although we shall essentially focus in the following on the case of the 87% porosity gel, for the sake of completeness we show in Fig. 1 the evolution of the simulated gel structure factor with porosity.

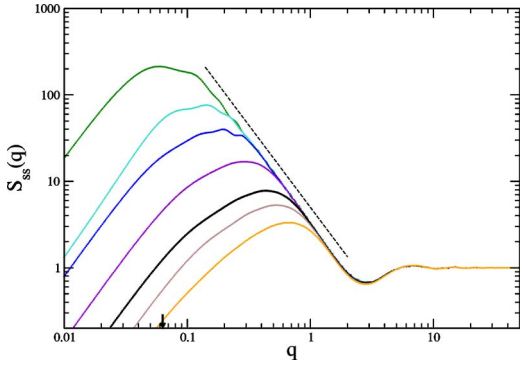

FIG. 1. (Color online) Gel structure factors $S_{gg}(q)$ obtained with the DLCA algorithm for different porosities. From left to right: $\phi=0.99,0.98,0.97,0.95,0.92,0.90,0.87$. The dashed line has a slope of -1.9. The arrow indicates the wave vector $q=2\pi/L\approx 0.063$ (q is in unit a^{-1}).

The curves closely resemble those obtained with the continuum model [18]. In particular, they exhibit the same damped oscillations at large q that result from the "extended" hard-core condition $g_{gg}(r)=0$ for $r<d$ (the oscillations, however, are more significant in the continuum model). The range of the linear fractal regime increases with porosity (it is almost nonexistent in the 87% gel) and corresponds asymptotically to a fractal dimension $d_f\approx 1.9$ (the value $d_f\approx 1.87$ was obtained in Ref. [1] from the $g_{gg}(r)$ plot for the 99% aerogel). A characteristic feature of the curves is the existence of a maximum at smaller wave vectors whose location q_m decreases with porosity and correlates well with $1/\xi_g$ ($q_m\sim 2.6/\xi_g$). This maximum is thus the Fourier-space signature of the shallow minimum observed in $g_{gg}(r)$. [Note that varying the size L has only a weak influence on the small q portion of the curves for the 87% and 95% gels, which validates the continuation procedure used in Eq. (5).]

To compute the scattering intensity $I(q)$ and compare to the results of small-angle x rays or neutron experiments, it would be necessary to introduce a form factor $F(q)$ for the gel particles. One could use, for instance, the form factor of spheres with radius $R=d/2$, $F(q)=3[\sin(qR)-qR\cos(qR)]/(qR)^3$. The curve $I(q)=S_{gg}(q)F(q)^2$ then differs from $S_{gg}(q)$ in the large-q regime ($q/2\pi>d^{-1}$) where it follows the Porod law $I(q)\sim q^{-4}$ [26]. On the other hand, the intermediate "fractal" regime ($\xi_g^{-1}<q/2\pi<d^{-1}$), where $S_{gg}(q)\sim q^{-d_f}$, and the location q_m of the maximum are essentially unchanged. By comparing the value of q_m in Fig. 1 with the actual value in the experimental curves (displayed for instance in Ref. [18]), we can thus fix approximately the scale of our coarse-graining. For $\phi=95\%$, $q_m\approx 0.01$ Å^{-1} which yields $a\approx 3$ nm, a reasonable value for base-catalysed silica aerogels which is in agreement with the estimation of Ref. [1] obtained from the gel correlation length ξ_g. It is worth noting that the DLCA simulated structure factors present a more pronounced maximum at q_m than the experimental curves $I(q)$, as already noticed in the literature [18,27]. There are obviously large scale inhomogeneities in actual aerogels that are not reproduced in the simulations. Moreover, as emphasized in Refs. [18,27], there are some significant details that are neglected in the DLCA model, such as the rotational diffusion of the aggregates, their polydispersity and irregular form, and all kinds of possible restructurating effects.

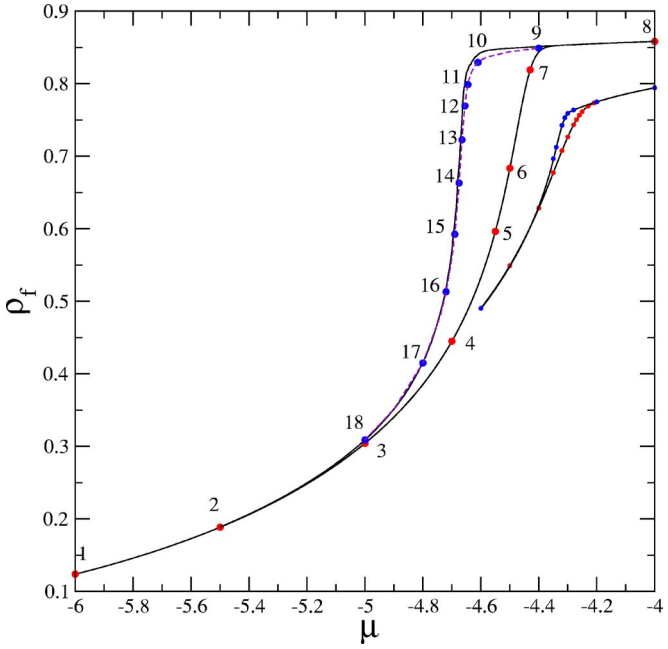

FIG. 2. (Color online) Average hysteresis loops in a 87% porosity aerogel at $T^*=0.5$ and 0.8 (from left to right). The points along the adsorption and desorption isotherms at $T^*=0.5$ indicate the values of the chemical potential for which the correlation functions are computed. The desorption isotherm has been computed either in the presence of an external reservoir (solid line) or by using the procedure described in Sec. III C (dashed line).

B. Fluid structure during adsorption

As shown in Refs. [1–3], the elementary condensation events (avalanches) that occur in 87% porosity aerogel as the chemical potential is slowly varied are always of microscopic size, whatever the temperature. This implies that the adsorption isotherms are smooth in the thermodynamic limit or when averaging over a large number of finite samples, as illustrated in Fig. 2. We have computed the correlation functions and the corresponding structure factors for a number of points along the $T^*=0.5$ and $T^*=0.8$ isotherms, as indicated in the figure. We first consider the lowest temperature.

Figures 3 and 4 show the evolution of the correlation functions $h_{ff}(r)$ and $h_{gf}(r)$ with chemical potential. One can see that the curves change significantly as μ increases [note that the vertical scale in Fig. 3(a) is expanded so as to emphasize the presence of a shallow minimum in the curves; accordingly, the values of $h_{ff}(r)$ near zero are not visible]. For very low values of the chemical potential (e.g., $\mu=-6$), $h_{ff}(r)$ looks very much like $h_{gg}(r)$, apart from a shift towards larger values of r by a distance of about 2 lattice spacings. Indeed, as shown in our earlier work [1,2], in the early stage of the adsorption process, the adsorbed fluid forms a liquid film that coats the aerogel strands and whose thickness is

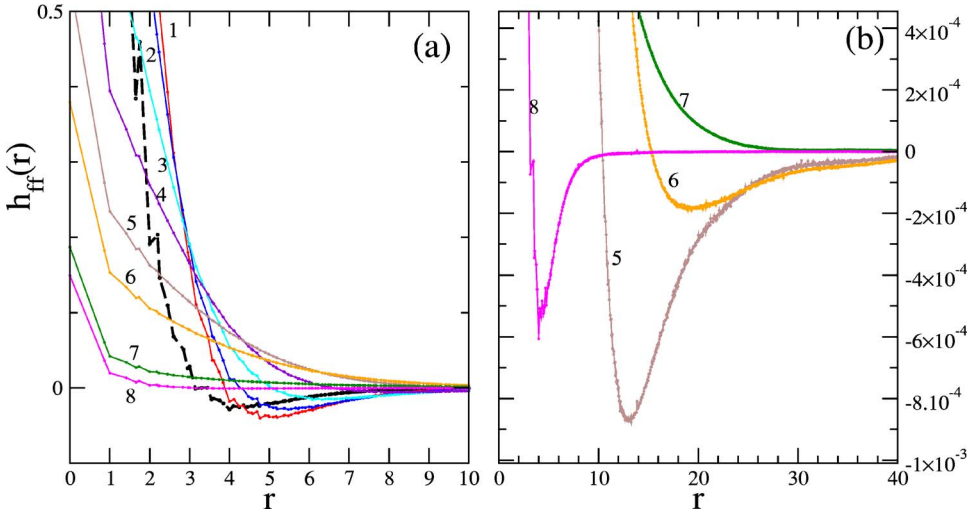

FIG. 3. (Color online) Fluid-fluid correlation function $h_{ff}(r)$ along the adsorption isotherm in a 87% porosity aerogel at $T^*=0.5$. (a) From top to bottom, the curves correspond to points 1–8 in Fig. 2; the dashed line is the gel correlation function $h_{gg}(r)$. (b) Magnification of (a) showing the evolution of the minimum as μ varies from −4.55 to −4 (points 5–8 in Fig. 2).

approximately one lattice spacing at low temperature. In consequence, the distribution of the fluid particles follows the spatial arrangement of the aerogel, a feature already observed in a continuum version of the model [28]. The existence of the liquid film also reflects in the rapid decrease of $h_{gf}(r)$ with r, which indicates that the fluid is only present in the vicinity of the gel particles [the fact that $h_{gf}(r=d) < h_{gf}(r=a)$ may be ascribed to the connectivity of the gel; around a gel particle, there are always other gel particles—2.5 in average in the first shell—and the probability to find a fluid particle is thus suppressed]. As μ increases, the magnitude of the fluid-fluid correlations decreases at small r (the contact value decreases from 4.45 to 0.15) and the depth of the minimum in $h_{ff}(r)$ decreases as it shifts to larger values of r (its location varies from 5 to 24 as μ increases from −6 to −4.47). The minimum disappears as the last voids in the gel fill with liquid [note the difference in the vertical scales of Figs. 3(a) and 3(b)], and finally, as one reaches saturation (at $\mu_{\text{sat}}=-4$), the shape of the gel-gel correlation function $h_{gg}(r)$ is recovered (together with its own minimum), in accordance with Babinet principle [26]. (This is not quite visible in Fig. 3 because of the drastic change in the vertical scales due to the factor $(1-\phi)^2/\phi^2$ [29].) A similar behavior is observed in the cross correlation function $h_{gf}(r)$ in Fig. 4, but the minimum occurs at a smaller distance [29].

As for $g_{gg}(r)$, we may associate to the location of the mimimum in $h_{ff}(r)$ a length ξ_f that characterizes the correlations within the adsorbed fluid (except close to saturation). The fact that ξ_f becomes significantly larger than ξ_g as the adsorption proceeds shows that the fluid develops its own complex structure that does not reflect anymore the underlying gel structure. This is likely in relation with the fact that some of the condensation events studied in our previous works [2,3] extend much beyond the largest voids in the aerogel [30]. It is worth noting that these large avalanches (with a radius of gyration $R_g \approx 12$ [2,3]) occur approximately in the same range of the chemical potential ($-4.5 \leqslant \mu \leqslant -4.4$) where ξ_f reaches its maximum (this also corresponds to the steepest portion of the isotherm).

The corresponding structure factors $S_{ff}(q)$ and $S_{gf}(q)$ are shown in Figs. 5 and 6, respectively [31]. The main feature in $S_{ff}(q)$ is the presence of a broad peak that grows and moves towards smaller wave vector as the fluid condenses in the porous space. This peak is clearly associated to the minimum in $h_{ff}(r)$ (its location is approximately proportional to ξ_f^{-1}) and it thus tells us the same story; the growing of a

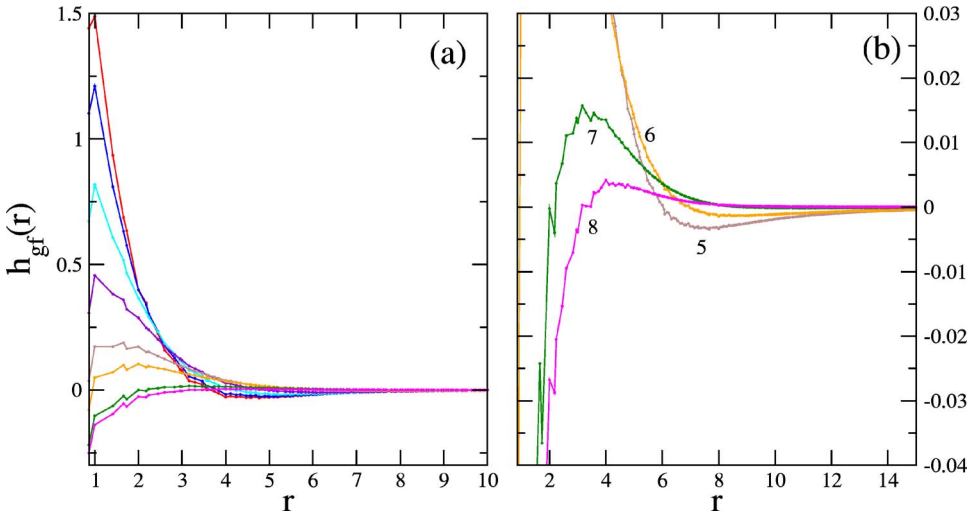

FIG. 4. (Color online) Same as Fig. 3 for the cross correlation function $h_{gf}(r)$.

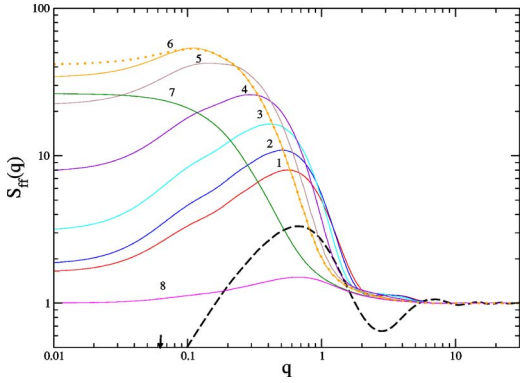

FIG. 5. (Color online) Fluid-fluid structure factor $S_{ff}(q)$ along the adsorption isotherm in a 87% porosity aerogel at $T^*=0.5$. The numbers refer to points 1–8 in Fig. 2. The dashed line is the gel structure factor $S_{gg}(q)$ and the dotted line illustrates the influence of the continuation procedure for $q<2\pi/L$ (see [31]).

characteristic length scale in the fluid along the capillary rise. The peak disappears in the last stage of the adsorption process and is then replaced by a plateau (see curve 7 in Fig. 5). Finally, at $\mu=\mu_{\text{sat}}$, one recovers a structure factor that can be deduced from $S_{gg}(q)-1$ by a linear transformation, in accordance with Babinet principle [there are no oscillations in $S_{ff}(q)$, however, because the fluid-fluid hard-core diameter is zero].

The evolution of the gel-fluid cross structure factor $S_{gf}(q)$ is somewhat different. The peak is more prominent, as a consequence of the "no-fluctuation" condition $S_{gf}(q=0)=0$ (this feature may not be so pronounced in actual systems because of large-scale fluctuations), and it is located at a larger wave vector than in $S_{ff}(q)$ [in line with the corresponding locations of the minima in $h_{ff}(r)$ and $h_{gf}(r)$]. The most substantial difference with $S_{ff}(q)$ is that the amplitude of the peak starts to decrease much before the end of the adsorption process. The negative correlation observed at saturation is again due to complementarity with the gel-gel structure [13].

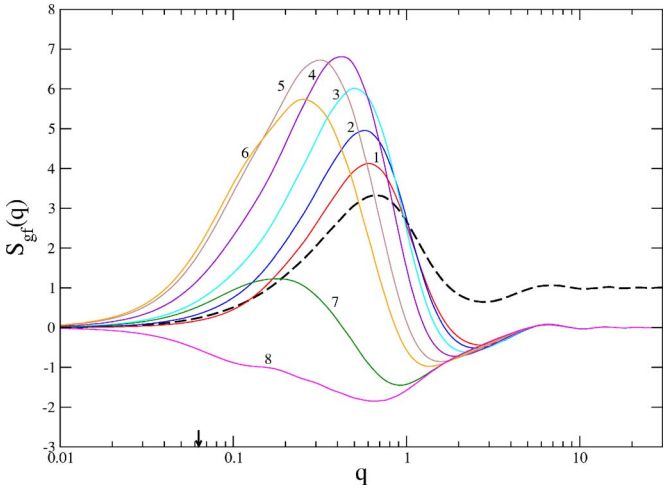

FIG. 6. (Color online) Same as Fig. 5 for the cross structure factor $S_{gf}(q)$. Note that the vertical scale is not logarithmic because $S_{gf}(q)$ has negative values.

We have repeated these calculations at $T^*=0.8$ in order to investigate the influence of temperature. In the 87% gel, $T^*=0.8$ is just below T_h, the temperature at which the hysteresis loop disappears (see Fig. 2). $h_{ff}(r)$ and $h_{gf}(r)$ still exhibit a minimum that moves towards larger r upon adsorption. However, the characteristic length ξ_f, associated to the minimum of $h_{ff}(r)$, does not exceed 14 lattice spacings, indicating that the size of the inhomogeneities in the fluid decreases with increasing T. A similar observation was made in Refs. [2,3] concerning the size of the avalanches which become more compact at higher temperature and often correspond to a condensation event occuring in a single cavity of the aerogel. The shape of the corresponding structure factors does not change significantly with respect to the $T^*=0.5$ case, but the amplitude is significanly reduced: the maximal amplitudes of the peaks in $S_{ff}(q)$ and $S_{gf}(q)$ are divided approximately by 5 and 2, respectively.

As shown in Refs. [1–3], temperature has a much more dramatic influence on the adsorption process in gels of higher porosity. In particular, at low enough temperature ($T<T_c(\phi)$ with $T_c^*(\phi)\approx 0.5$ in the 95% gel [3]), a macroscopic avalanche occurs at a certain value of the chemical potential, with the whole sample filling abruptly, which results in a discontinuous isotherm in the thermodynamic limit. In a finite system, the signature of a macroscopic avalanche is a large jump in the fluid density whose location in μ fluctuates from sample to sample, which results in a steep but smooth isotherm after an average over the gel realizations (one then has to perform a finite-size scaling study to conclude on the proper behavior in the thermodynamic limit [1,3]). Within a grand canonical calculation, there is unfortunately no way to study the evolution of the structural properties of the fluid during a macroscopic avalanche as this would require us to consider intermediate fluid densities that are inaccessible [32] (the situation would be different if the fluid density was controlled instead of the chemical potential, as is done frequently in experiments [6,33]). All we can do is to study the 95% gel at a higher temperature where the adsorption is still gradual, for instance at $T^*=0.8$. In this case, no qualitative change is found with respect to the case of the 87% gel at $T^*=0.5$. Indeed, as emphasized in Ref. [3], adsorption proceeds similarly in a high-porosity gel at high temperature and in a lower-porosity gel at low temperature. The correlation length ξ_f is somewhat larger in the 95% gel (beyond 30 lattice spacings) so that finite-size effects come into play [in particular, it becomes problematic to extraplotate $S_{ff}(q)$ to $q=0$ so as to simulate the infinite-size limit]. To go to lower temperatures, it would be thus necessary to use a much larger simulation box, which would increase considerably the computational work. Note that one expects $h_{ff}(r)$ to decay algebraically at the critical temperature $T_c(\phi)$. Indeed, according to the analogy with the $T=0$ nonequilibrium random-field Ising model (RFIM), there should be only one important length scale in the system close to criticality, length scale which is proportional to the average linear extent of the largest avalanches [34]. At criticality, this correlation length diverges.

C. Fluid structure during desorption

As discussed in detail in Refs. [1,2], different mechanisms may be responsible for gas desorption in aerogels, depending

on porosity and temperature. In contrast with adsorption, the outer surface of the material where the adsorbed fluid is in contact with the external vapor may play an essential role. For instance, in the 87% aerogel at $T^*=0.5$, the theory predicts a phenomenon akin to percolation invasion, as μ is decreased from saturation, some gas "fingers" enter the sample and grow until they percolate at a certain value of μ, forming a fractal, isotropic cluster. The desorption then proceeds gradually via the growth of the gaseous domain. Accordingly, in the thermodynamic limit, the isotherm shows a cusp at the percolation threshold followed by a steep but continuous decrease (the cusp is rounded in finite samples).

The simulation of the desorption process thus requires the use of an explicit external reservoir adjacent to the gel sample, which of course introduces a severe anisotropy in the model and makes it difficult to calculate radially averaged correlation functions. To circumvent this problem, we have used another procedure where the desorption is not initiated by the interface with an external reservoir but triggered by the presence of gas bubbles inside the material. We have indeed observed in our previous studies (see Fig. 16 in Ref. [1]) that the last desorption scanning curves (obtained by stopping the adsorption just before saturation and then decreasing the chemical potential) look very much like the desorption isotherms obtained in presence of a reservoir (when averaging the fluid density deep inside the aerogel, which gives a good estimate of the isotherm that would be obtained in the limit $L\to\infty$). Near the end of the adsorption process, the remaining gaseous domain is composed of isolated bubbles which obviously play the same role as an external reservoir when the chemical potential is decreased. The advantage of initiating the desorption with these last bubbles is that one can use the same geometry as during adsorption, with periodic boundary conditions in all directions (moreover, using small bubbles instead of a planar interface of size L^2 considerably suppresses finite-size effects).

In practice, the calculation has been performed by keeping five bubbles in each sample. This implies that the chemical potential at which desorption is initiated is slightly different in each sample (if one chooses the same μ in all samples, some of them may be already completely filled with liquid). This number of bubbles results from a compromise: on the one hand, keeping a single bubble may not be sufficient to trigger the desorption process (in some samples, the growth of the bubble is hindered by the neighboring gel particles and the desorption occurs at a much lower value of the chemical potential); on the other hand, keeping too many bubbles results in a too rapid growth of the gas domain. As can be seen in Fig. 2, the isotherm obtained with this procedure is indeed very close to the isotherm calculated in presence of an external reservoir.

The fluid-fluid and solid-fluid correlation functions computed at several points along the desorption branch are shown in Figs. 7 and 8.

One can see that $h_{ff}(r)$ is dramatically changed with respect to adsorption; from saturation down to $\mu\approx-4.7$ (curves 9–16), the function is monotonically decreasing, showing no minimum. Moreover, as shown in the inset of Fig. 7, a long-range tail is growing and $h_{ff}(r)$ may differ significantly from zero at $r=L/2$ [36]. Although it is difficult

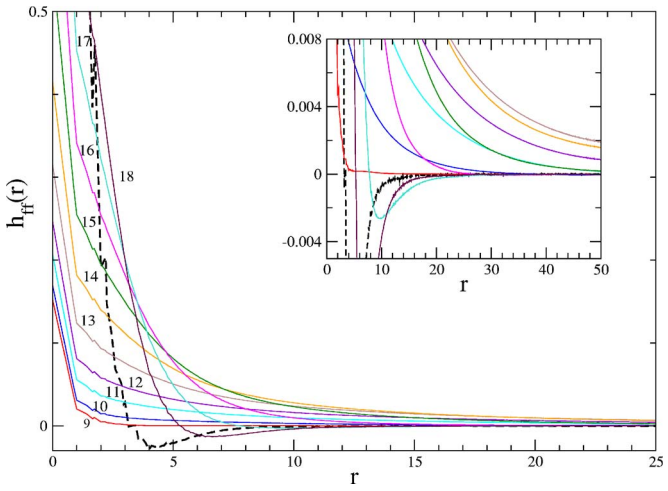

FIG. 7. (Color online) Fluid-fluid correlation function $h_{ff}(r)$ along the desorption isotherm in a 87% porosity aerogel at $T^*=0.5$. The numbers refer to the points in Fig. 2; the dashed line is the gel correlation function $h_{gg}(r)$. The vertical scale is expanded in the inset, showing the very slow decrease of $h_{ff}(r)$ towards zero in the steepest portion of the isotherm.

to characterize this decrease by a unique and well-defined correlation length (the curve cannot be fitted by a simple function such as an exponential), it is clear that the range of the correlations is small at the beginning of the desorption process, then increases considerably, goes through a maximum in the steeppest portion of the isotherm (corresponding approximately to point 13 in Fig. 2), and eventually decreases. As the hysteresis loop closes and the adsorbed phase consists again of a liquid film coating the areogel strands, a shallow minimum reappears in the curve, which is reminiscent of the underlying gel structure.

In contrast, the changes in the cross-correlation function $h_{gf}(r)$ between adsorption and desorption are very small (the function has only a slightly longer tail during desorption). It appears that the gel-fluid correlations depend essentially on the average fluid density; for a given value of ρ_f, they are almost the same on the two branches of the hysteresis loop.

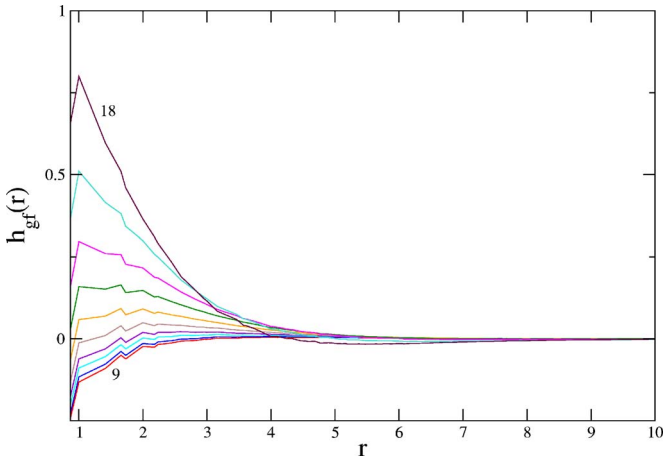

FIG. 8. (Color online) Same as Fig. 7 for the cross correlation function $h_{gf}(r)$.

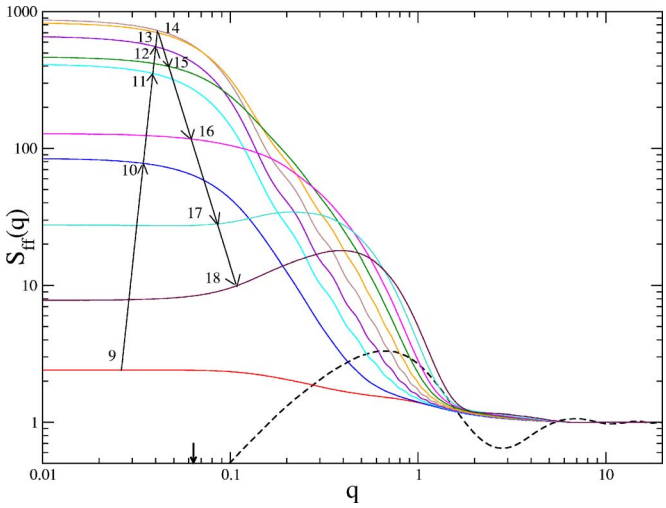

FIG. 9. (Color online) Fluid-fluid structure factor $S_{ff}(q)$ along the desorption isotherm in a 87% porosity aerogel at $T^*=0.5$. The numbers and arrows refer to points 9–18 in Fig. 2. The dashed line is the gel structure factor $S_{gg}(q)$.

The calculation of the fluid-fluid structure factor $S_{ff}(q)$ is complicated by the fact that $h_{ff}(r)$ decreases very slowly to zero, and one cannot use anymore the continuation procedure that forces the sum rule, Eq. (11), to be satisfied (the results for $q<2\pi/L$ change considerably with L, which shows that the resulting curve is not a good approximation of the infinite size limit). Instead, we have only subtracted from $h_{ff}(r)$ its value at $r=L/2$ [setting $h_{ff}=h_{ff}(r=L/2)$ in Eq. (12)] so as to avoid the large but spurious oscillations in $S_{ff}(q)$ that result from the discontinuity at $L/2$ [there is still a discontinuity in the slope of $h_{ff}(r)$ at $L/2$ that induces small oscillations in some of the curves of Fig. 9]. It is clear that finite-size effects are important in this case and the results for $q<2\pi/L$ must be considered with caution.

The resulting fluid-fluid structure factors along the desorption isotherm are shown in Fig. 9. [We do not present the curves for $S_{gf}(q)$ as they look very much like those in Fig. 6 with only a slightly broader peak.] As could be expected, the structure factors computed just before and after the knee in the isotherm (for $\mu>-4.67$) are very different from those obtained during adsorption. First, the peak that was associated to the minimum in $h_{ff}(r)$ has now disappeared and the small-q intensity saturates to a value that is considerably larger than the maximum value obtained during adsorption (compare the vertical scales in Figs. 5 and 9). Secondly, as μ varies from −4.65 to −4.67 (curves 11–14), there is a linear portion in $S_{ff}(q)$ whose maximal extension is about one decade on a log-log scale. On the other hand, when μ is decreased further, the peak in $S_{ff}(q)$ is recovered and the curves become more similar to the ones computed on the adsorption branch.

The linear regime in $S_{ff}(q)$ strongly suggests the presence of fractal correlations [35]. However, according to our previous studies [2], it is only the *gaseous* domain that should be a fractal object at the percolation threshold, as illustrated by the isotropic and strongly ramified structure shown in Fig. 10. The correlation function $h_{ff}(r)$, on the other hand, does

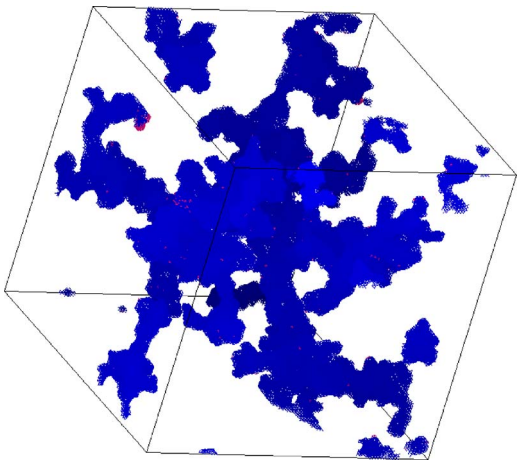

FIG. 10. (Color online) Snapshot of the vapor domain in a 87% gel sample during desorption at $T^*=0.5$ and $\mu=-4.63$.

not discriminate between a site representing a gaseous region ($\rho_i\approx 0$ at low temperature) and a site representing a gel particle ($\rho_i\equiv 0$). In order to really show the existence of fractal correlations within the gas domain, one must consider either the "gas-gas" correlation function (defining the quantity $\rho_i^{\text{gas}}=\eta_i-\rho_i$ which is equal to 1 only in the gas phase) or the complementary function that measures the correlations within the dense (solid or liquid) phase (one then defines $\rho_i^{\text{dense}}=1-\rho_i^{\text{gas}}$). The corresponding structure factor $S_{dd}(q)$ is the quantity that is measured experimentally when using the "contrast matching" technique [7]. It is related to $S_{ff}(q)$ and $S_{gf}(q)$ by

$$(\rho_g+\rho_f)(S_{dd}(q)-1)=\rho_f(S_{ff}(q)-1)+\sqrt{\rho_g\rho_f}S_{gf}(q)+\rho_g(S_{gg}(q)-1). \tag{15}$$

$S_{dd}(q)$ is shown in Fig. 11 for $\mu=-4.65$ [37], in the region of the knee in the desorption isotherm (point 11 in Fig. 2). It clearly contains a linear portion over almost one decade and can be very well represented in this range of wave vectors by the fit [38]

$$S_{dd}(q)\sim\frac{\sin[(d_f-1)\tan^{-1}(ql)]}{q[l^{-2}+q^2]^{(d_f-1)/2}} \tag{16}$$

with $d_f=2.45$ and $l=17$, where l is a crossover length that limits the fractal regime at large distances. Note that the linear portion itself has a slope ≈ -2.1 (the above formula reproduces the right slope only when l is very large [18]). An accurate determination of d_f would therefore require a much larger system and, at this stage, it is not possible to decide if the fractal dimension is consistent with that of random percolation. In any case, these results strongly suggest that the gas domain exhibits fractal correlations during desorption, correlations which have no relation with the underlying gel microstructure (we recall that there is almost no fractal regime in the 87% aerogel, as can be seen in Fig. 1).

Raising the temperature to $T^*=0.8$ has a dramatic effect, as shown in Fig. 12. The maximum value of $S_{ff}(q)$ has dropped by two orders of magnitude and there is no significant region with a fractal-like power-law behavior. Indeed,

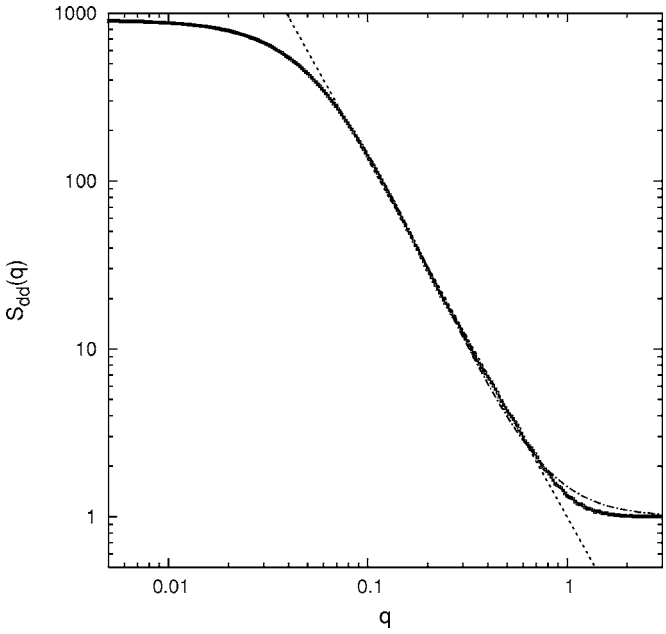

FIG. 11. Structure factor of the dense phase (see text), $S_{dd}(q)$, during desorption at $T^*=0.5$ and $\mu=-4.65$. The dashed-dotted curve is the best fit according to Eq. (16) and the straight dashed line has a slope of −2.1.

$h_{ff}(r)$ has no more a long-range tail and the correlations are very similar during adsorption and desorption, as could be expected from the very thin shape of hysteresis loop. This is the signature that the desorption mechanism has changed, in agreement with the analysis of Refs. [1] and [2]. It is now due to a cavitation phenomenon in which gas bubbles first appear in the largest cavities of the gel and then grow and coalesce until the whole void space is invaded [39].

We have not studied the correlations during desorption in the 95% porosity gel. At very high temperature ($T^* \gtrsim 0.9$), desorption is expected to be due again to cavitation [2], and the results shoud be similar to those in the 87% that have just been described. On the other hand, at low temperature (e.g., $T^*=0.5$), the theory predicts a depinning transition in which a self-affine interface sweeps through the whole sample, resulting in a discontinuous desorption isotherm [2]. Therefore, like in the case of the macroscopic avalanche during adsorption, the correlations along the isotherm cannot be studied within the framework of a grand-canonical calculation. At intermediate temperatures, one could probably observe again extended fractal correlations associated with a percolating cluster of gas, but this study requires the use of larger systems so as to probe smaller values of q and discriminate the effects due to the own fractal structure of the gel.

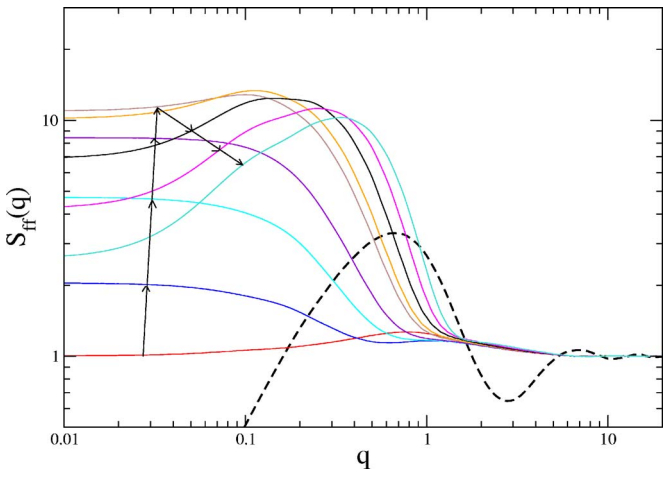

FIG. 12. (Color online) Fluid-fluid structure factor $S_{ff}(q)$ along the desorption isotherm in a 87% porosity aerogel at $T^*=0.8$.

IV. SCATTERED INTENSITY AND COMPARISON WITH EXPERIMENTS

As mentioned in the Introduction, there have been two recent scattering studies of gas condensation in aerogels, both with ^{4}He [8,9]. In Ref. [9], light scattering is used to study adsorption and desorption in a 95% porosity gel at several temperatures between 4.47 K ($T^* \approx 0.86$) and 5.08 K ($T^* \approx 0.98$). These experimental results cannot be directly compared to our theoretical predictions, and our system size is too small to investigate the large-scale inhomogeneities that are seen in the experiments (some of them are visible to the eye). However, there are two key observations that appear to be in agreement with our predictions: (i) at the lowest temperature studied, the optical signal due to helium adsorption is larger than if the fluid density was simply correlated to the density of silica, indicating that the correlations within the fluid extend beyond the aerogel correlation length, and (ii) the aerogel is much brighter during desorption, indicating that the characteristic size of the density fluctuations is much larger than during adsorption.

This latter conclusion was also reached from the small-angle x-ray scattering measurements (SAXS) performed in a 98% porosity aerogel at 3.5 K ($T^* \approx 0.67$) [8]. SAXS is particularly well suited for observing the structural features associated with fluid adsorption, and in order to compare more easily to experiments we shall push further our calculations and compute the resulting scattered intensity. Of course, the predictions must be taken with a grain of salt, considering the limitations in the model and the theory. Since the scattered intensity is proportional to the Fourier transform of the electron density fluctuations, one has

$$I(q) \propto \rho_g F(q)^2 S_{gg}(q) + 2\sqrt{\rho_g \rho_f}\alpha F(q) S_{gf}(q) + \rho_f \alpha^2 S_{ff}(q), \tag{17}$$

where $F(q)$ is the form factor of silica particles (see Sec. III A) and α is the ratio of the electron density in the adsorbed fluid to that in the solid. As an additional approximation, we shall take $F(q) \approx 1$, restricting the study to the range $2\pi/L \leqslant q \leqslant 2$ where this is presumably a reasonable approximation (in real units this corresponds to $0.02 \lesssim q \lesssim 0.7$ nm^{-1}, taking $a=3$ nm). Assuming that the adsorbed liquid has the same density as the bulk liquid at P_{sat}, and using the tabulated densities of helium and silica, one finds that α varies from 6.55×10^{-2} at $T^*=0.5$ to 5.75×10^{-2} at $T^*=0.8$.

The theoretical scattered intensities during adsorption and desorption in the 87% gel at $T^*=0.5$ are shown in Figs. 13

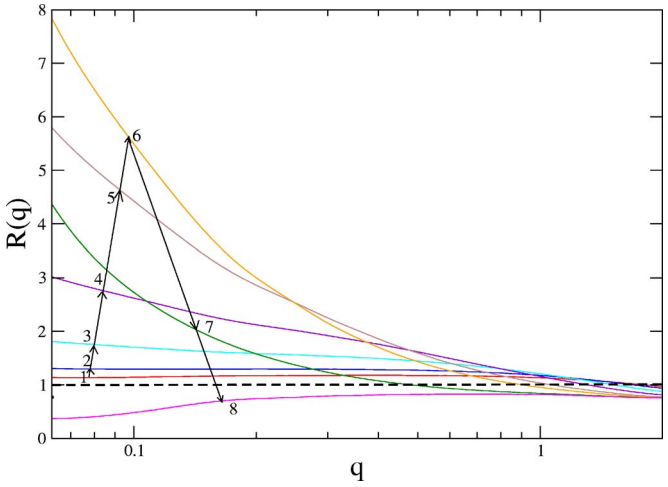

FIG. 13. (Color online) Theoretical ratio $R(q)$ of the scattered intensity $I(q)$ to the scattered intensity $I_e(q)$ of the empty aerogel during helium adsorption in a 87% aerogel at $T^*=0.5$. The dashed line corresponding to $R=1$ is shown for reference.

and 14. As in the experiments [8], we plot the ratio $R(q)=I(q)/I_e(q)$, where $I_e(q)$ is the contribution of the empty aerogel [the first term on the right-hand side of Eq. (17)] in order to accentuate the effects of the adsorbed gas, especially in the initial stage of adsorption. Moreover, we hope that this also partially corrects the small-q defects due to the absence of large-scale fluctuations in the DLCA gel structure factor.

The main features of the curves displayed in Fig. 13 are the following: (i) At the very beginning of adsorption, $R(q)$ slightly increases but remains almost independent of q. This is the signature of the ^{4}He film coating the aerogel. In this regime, the main contribution to the scattered intensity comes from the gel-fluid correlations [the second term on the right-hand side of Eq. (17)]. (ii) As μ increases, the scattering grows in intensity at small q, reflecting the presence of the broad peak in $S_{ff}(q)$ that moves towards a smaller wave vector with filling (see Fig. 5). (iii) As the aerogel fills further, $R(q)$ decreases again until it becomes almost flat at complete filling. The total intensity is then reduced with respect to that of the empty aerogel. Direct comparison with the experimental results of Ref. [8] is again problematic; the adsorption isotherm in the 98% gel is indeed very steep at 3.5 K, suggesting that one may be in the regime of a macroscopic avalanche. However, the behavior of the experimental $R(q)$ is remarkably similar to what has just been described (preliminary measurements in a 86% aerogel [40] also show the same trends). The results of Ref. [8] were interpreted according to a model of two-phase coexistence, with a "film" phase in equilibrium with a filled "pore" phase. This is at odds with the theoretical scenario discussed in Refs. [1–3] which emphasizes the nonequilibrium character of the transition. The present results seem to show that this approach can also elucidate (at least qualitatively) the behavior of the scattered intensity.

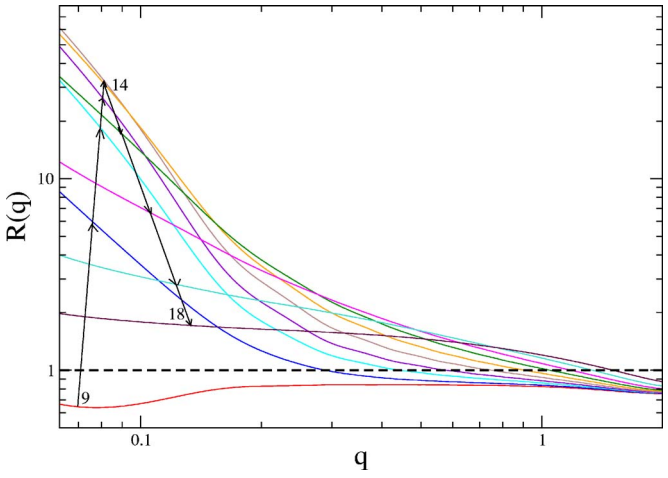

FIG. 14. (Color online) Same as Fig. 13 during desorption.

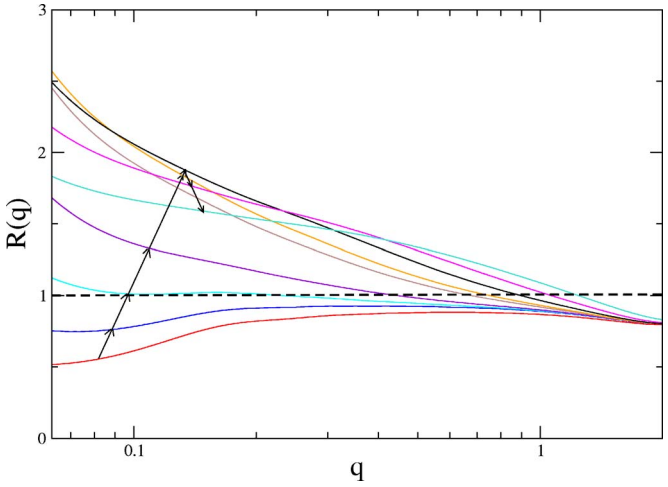

FIG. 15. (Color online) Same as Fig. 13 during desorption at $T^*=0.8$.

During desorption, the most characteristic feature of the curves shown in Fig. 14 is the very significant increase of the ratio $R(q)$ at small q with respect to adsorption (note the logarithmic scale on the vertical axis). This is related to the corresponding increase in $S_{ff}(q)$ shown in Fig. 9 and is clearly due to the presence of long-range correlations within the fluid. As the desorption proceeds, $R(q)$ goes through a maximum and then decreases until it becomes flat again. Remarkably, no power-law fractal regime is visible in $R(q)$ in the range $0.06 \lesssim q \lesssim 1$ as was the case with $S_{dd}(q)$ in Fig. 11. It is the small value of α (due to the small electron density of He), and not the division by $I_e(q)$, which is responsible for this unfortunate disappearance [$I(q)$ becomes proportional to $S_{dd}(q)$ when $\alpha=1$, which is only the case in a contrast matching experiment]. In the measurements of Ref. [8], this increase of $R(q)$ at small q is not mentionned, but the analysis of the data shows that the charateristic size of the inhomogeneities is much larger than during adsorption, as already mentioned, and that it decreases rapidly in the last stage of desorption.

Not surprisingly, the theoretical scattered intensity in the 87% aerogel is considerably smaller at high temperature, as illustrated in Fig. 15 for $T^*=0.8$. The intensity ratio $R(q)$ has been divided by about 40. We therefore conclude that the

magnitude of the scattered intensity can indicate that the nature of the desorption process has changed. We leave to our colleague experimentalists the challenge of checking the presence of a fractal-regime during desorption, as was done in Vycor [10–12] and xerogel [14].

ACKNOWLEDGMENTS

We are grateful to N. Mulders for very useful discussions and communication of unpublished results. The Laboratoire de Physique Théorique de la Matière Condensée is the UMR 7600 of the CNRS.

[1] F. Detcheverry, E. Kierlik, M. L. Rosinberg, and G. Tarjus, Phys. Rev. E **68**, 061504 (2003).
[2] F. Detcheverry, E. Kierlik, M. L. Rosinberg, and G. Tarjus, Langmuir **20**, 8006 (2004).
[3] F. Detcheverry, E. Kierlik, M. L. Rosinberg, and G. Tarjus, cond-mat/0508267, Phys. Rev. E **72**, 051506 (2005).
[4] S. J. Gregg and K. S. W. Sing, *Adsorption, Surface Area, and Porosity* (Academic, New York, 1982).
[5] M. H. W. Chan, Czech. J. Phys. **S6**, 2915 (1996).
[6] D. J. Tulimieri, J. Yoon, and M. H. W. Chan, Phys. Rev. Lett. **82**, 121 (1999).
[7] For a recent review, see, e.g., E. Hoinkis, Part. Part. Syst. Charact. **21**, 80 (2004).
[8] L. B. Lurio, M. Mulders, M. Paerkau, M. Lee, S. G. J. Mochrie, and M. H. W. Chan, J. Low Temp. Phys. **121**, 591 (2000).
[9] T. Lambert, C. Gabay, L. Puech, and P. E. Wolf, J. Low Temp. Phys. **134**, 293 (2004); T. Lambert, Ph.D. thesis, Université Joseph Fourier, Grenoble I (2004).
[10] J. C. Li, D. K. Ross, L. D. Howe, K. L. Stefanopoulos, J. P. A. Fairclough, R. Heenan, and K. Ibel, Phys. Rev. B **49**, 5911 (1994).
[11] J. H. Page, J. Liu, B. Abeles, E. Herbolzheimer, H. W. Deckman, and D. A. Weitz, Phys. Rev. E **52**, 2763 (1995).
[12] A. Ch. Mitropoulos, J. M. Haynes, R. M. Richardson, and N. K. Kanellopoulos, Phys. Rev. B **52**, 10035 (1995); E. S. Kikkinides, M. E. Kainourgiadis, K. L. Stefanopoulos, A. Ch. Mitropoulos, A. K. Stubos, and N. K. Kanellopoulos, J. Chem. Phys. **112**, 9881 (2000).
[13] R. Salazar and L. D. Gelb, Mol. Phys. **102**, 1015 (2004).
[14] E. Hoinkis and B. Röhl-Kuhn, in *Fundamental of Adsorption 7*, edited by K. Kaneko, H. Kanoh, and Y. Hanzawa (IK International, Japan, 2002).
[15] P. Meakin, Phys. Rev. Lett. **51**, 1119 (1983); M. Kolb, R. Botet, and R. Jullien, *ibid.* **51**, 1123 (1983).
[16] E. Kierlik, P. A. Monson, M. L. Rosinberg, L. Sarkisov, and G. Tarjus, Phys. Rev. Lett. **87**, 055701 (2001); E. Kierlik, P. A. Monson, M. L. Rosinberg, and G. Tarjus, J. Phys.: Condens. Matter **14**, 9295 (2002); M. L. Rosinberg, E. Kierlik, and G. Tarjus, Europhys. Lett. **62**, 377 (2003); F. Detcheverry, E. Kierlik, M. L. Rosinberg, and G. Tarjus, Adsorption **11**, 115 (2005).
[17] H. J. Woo, L. Sarkisov, and P. Monson, Langmuir **17**, 7472 (2001); L. Sarkisov and P. A. Monson, Phys. Rev. E **65**, 011202 (2001); H. J. Woo and P. A. Monson, *ibid.* **67**, 041207 (2003).
[18] A. Hasmy, E. Anglaret, M. Foret, J. Pelous, and R. Jullien, Phys. Rev. B **50**, 6006 (1994).
[19] A. Meroni, D. Levesque, and J. J. Weis, J. Chem. Phys. **105**, 1101 (1996).
[20] J. A. Given and G. Stell, J. Chem. Phys. **97**, 4573 (1992).
[21] M. L. Rosinberg, G. Tarjus, and G. Stell, J. Chem. Phys. **100**, 5172 (1994).
[22] From Eq. (2) (with μ replaced by μ_i), one obtains the equation $\mathcal{G}_{ff}(\mathbf{r}_{ij})=\rho_i(\eta_i-\rho_i)/\eta_i[\delta_{\mathbf{r}_{ij},\mathbf{0}}+\beta\Sigma_{k/i}\mathcal{G}_{ff}(\mathbf{r}_{kj})]$, where $\mathcal{G}_{ff}(\mathbf{r}_{ij}) \equiv \partial^2\beta\Omega^{\mathrm{eq}}/(\partial\beta\mu_i\partial\beta\mu_j)=\rho_f^2 h_{ff,c}(\mathbf{r}_{ij})+\rho_f\delta_{\mathbf{r}_{ij},\mathbf{0}}$, and the sum runs over the nearest neighbors of site i. This equation must be solved by iteration for every $\mathbf{r}_{ij}$, a very demanding numerical task in general [see, e.g., in a different context, D. Lancaster, E. Marinari, and G. Parisi, J. Phys. A **28**, 3959 (1995)].
[23] Note that this issue is not discussed in Ref. [13].
[24] Strictly speaking, this is only true at equilibrium, where Eq. (10) holds (see the equation just above in [22]). In particular, the fluid isothermal compressibility χ given by $k_BT\rho_f\chi=1+\rho_f\Sigma_{\mathbf{r}}h_{ff,c}(\mathbf{r})$ [21] is very small at low temperature. It would be worth checking by Monte Carlo simulations that $h_{ff,d}(\mathbf{r})$ is the most important contribution to $h_{ff}(\mathbf{r})$ along the sorption isotherms too. Note that in random-field-like systems these disorder-induced fluctuations are expected to be also predominant near criticality, with $h_{ff,d}(\mathbf{r})$ diverging more strongly than $h_{ff,c}(\mathbf{r})$ [see, e.g., E. Pitard, M. L. Rosinberg, G. Stell, and G. Tarjus, Phys. Rev. Lett. **74**, 4361 (1995)].
[25] On the other hand, a box of size $L=200$ has been used to simulate the aerogels with porosity $\phi\geqslant 0.97$.
[26] G. Porod, *Small Angle X-Ray Scattering* (Academic, London, 1982).
[27] N. Olivi-Tran and R. Jullien, Phys. Rev. B **52**, 258 (1995).
[28] V. Krakoviack, E. Kierlik, M. L. Rosinberg, and G. Tarjus, J. Chem. Phys. **115**, 11289 (2001).
[29] According to the Babinet principle, two "complementary" objects have the same diffraction properties. When the gel is completely filled with a liquid whose density is approximately uniform and close to 1 (which is the case at low temperature), the Babinet principle (in real space) implies that $h_{ff}(r)\approx(1-\phi)^2/\phi^2 h_{gg}(r)$ and $h_{gf}(r)\approx-(1-\phi)/\phi h_{gg}(r)$.
[30] The size of a so-called "void" or "cavity" in the lattice aerogel may be estimated from the radius of the largest sphere that can be inserted in the cavity without overlapping with a gel site [13] [see also L. D. Gelb and K. E. Gubbins, Langmuir **15**, 305 (1999)]. Alternatively, one can compute an integer "distance" n associated with the length of the shortest path from an empty site to a gel site [1]. The two procedures gives similar results. For a 87% aerogel, the size of the largest cavity is $n\approx 5$ which is comparable to the correlation length ξ_g.
[31] We recall that $S_{ff}(q)$ has been computed so as to satisfy Eq. (11), the correct $q=0$ limit of $h_{ff,d}(q)$. Then $S_{ff}(q)$ is expected to represent more faithfully the structure factor of the infinite system. In fact, setting $h_{ff}=0$ or $\neq 0$ in Eq. (12) only changes $S_{ff}(q)$ for $q\lesssim 2\pi/L$ and the differences are small, as illustrated by the dotted curve in Fig. 5. The same is true for $S_{gf}(q)$.
[32] One could imagine to separately study the samples in which

the jump has not yet occured and those which are already in the high-density phase, and then to use a sort of "lever" rule to compute the structural properties at intermediate densities. However, this would be an incorrect procedure: the two fluid configurations before and after the avalanche are not in equilibrium (they are both metastable and the grand-potential has decreased during the avalanche) and one cannot apply to this problem the standard methods of phase equilibria.

[33] A. P. Y. Wong and M. H. W. Chan, Phys. Rev. Lett. **65**, 2567 (1990).

[34] K. Dahmen and J. P. Sethna, Phys. Rev. B **53**, 14872 (1996); J. P. Sethna, K. Dahmen, and O. Perković, in *The Science of Hysteresis*, edited by G. Bertotti and I. Mayergoyz (Elsevier, New York, 2004).

[35] This important feature has not been observed in the study of Ref. [13]. This is perhaps due to the fact that the system size is too small; a cubic lattice of size $L=256$ is used, but since the gel particle radius is at least equal to 2 lattice spacings, the ratio L/d is smaller than in our simulations.

[36] This can be understood by noting that Eq. (9) can be rewritten as $\rho_f^2 h_{ff,d}(\mathbf{r})=(1/N)\Sigma_{i,j}[\overline{\delta\rho_i\delta\rho_j}+\overline{\rho_f^2(\{\eta_i\})}-\rho_f^2]\delta_{\mathbf{r},\mathbf{r}_{ij}}$ where $\delta\rho_i=\rho_i-\rho_f(\{\eta_i\})$ represents the deviation of ρ_i from the average density in the sample. The term $\overline{\rho_f^2(\{\eta_i\})}-\rho_f^2$ is of order $1/N$ but it may be not negligible in a finite system when the number of fluid particles fluctuates significantly from one sample to another. It may then dominate the long-range behavior of $h_{ff,d}(\mathbf{r})$. This is precisely what happens in the steepest portion of the desorption isotherm where some samples are still filled with liquid whereas other ones are already significantly drained.

[37] The structure factor $S_{dd}(q)$ shown in Fig. 11 has been computed from the Fourier transform of the "dense-dense" correlation function $h_{dd}(\mathbf{r})$, using a fit of the form $h_{dd}(\mathbf{r})\sim\exp(-r/l)/r^{3-d_f}$ to extrapolate the function to $r>L/2$. This procedure is used to avoid the small oscillations that come from $S_{ff}(q)$ and $S_{gf}(q)$ when $S_{dd}(q)$ is directly computed from Eq. (15).

[38] T. Freltoft, J. K. Kjems, and S. K. Sinha, Phys. Rev. B **33**, 269 (1986).

[39] Accordingly, the outer surface of the material does not play a role anymore [1,2] and one can study the correlation functions along the desorption isotherm without introducing an explicit external reservoir or using the last remaining gas bubbles. One can also safely extrapolate $S_{ff}(q)$ towards $q=0$ since there are no long-range correlations.

[40] N. Mulders (private communication).